Study of the dynamic interaction between planetary vehicles and planets soft soil

Hassan Shibly*

Robotics and Mechatronics,
School of Engineering, Science, and Technology,
Central Connecticut State University,
1615 Stanley Street, New-Britain, CT 06050, USA
Email: hshibly@ccsu.edu
*Corresponding author

Nidal Al-Masoud

Mechanical Engineering,
School of Engineering, Science, and Technology,
Central Connecticut State University,
1615 Stanley Street, New-Britain, CT 06050, USA
Email: almasoudn@ccsu.edu

Abstract: This paper examines expanding the range of manoeuvrability, ease of motion and improving the mobility system of Mars rovers. The focus of the research is on the enhancement of rover's speed and mobility under numerous constraints imposed by rugged and difficult-to-navigate terrains that include abrupt change of ground level, soft soil, obstacles and rocks. The article presents a study and simulation of the dynamic response of a free fall of a quarter vehicle model with rigid wheel on a soft soil. A simplified form of Bekker's equation is incorporated in the numerical solution of the governing equations of motion. The response of the dynamic interaction of rigid wheel and soft soil has three stages: sinkage stage, equilibrium stage and pullout from soil stage. The rigid body mode of the dynamic response is required to let the sprung mass pullout the rigid wheel from soft soil. The simulation results demonstrate that the first three stages of the first fall are the most significant. They have larger sinkage, larger resistance force and larger amplitude of dynamic response. The existence of damping reduces the magnitudes and prevents the unsprung mass from pulling out the wheel from the soil. The normal force on the rigid wheel for this case can be approximated and replaced by a triangle-shaped distribution. The simulations results conform to the theoretical counterparts.

Keywords: dynamic modelling; dynamic response; equivalent sinkage resistance; interaction with soft soil; nonlinear soil resistance; rigid wheel-soil sinkage; sinkage by free fall; soft soil resistance; stages of rigid wheel soil interaction.

Reference to this paper should be made as follows: Shibly, H. and Al-Masoud, N. (2017) 'Study of the dynamic interaction between planetary vehicles and planets soft soil', *Int. J. Mechanisms and Robotic Systems*, Vol. 4, No. 1, pp.61–79.

Biographical notes: Hassan Shibly received his PhD in Mechanical Engineering, Robotics and Control, at Carnegie Mellon University, USA. He is an Associate Professor of Robotics and Mechatronics at Central Connecticut State University, USA. His current research areas of interest include mobile robots and their interaction with ground soil.

Al-Masoud received his PhD in Mechanical Engineering from University at Buffalo, The State University of New York in 2002. He is currently a Professor of Mechanical Engineering at Central Connecticut State University, USA. His doctoral research was in Active Control of Thermo-Acoustic Instabilities. His main area of research is in modelling and control of dynamic systems.

1 Introduction

Driving planetary exploration rovers across the surface of the planet is an extremely challenging and complicated operation. Although the mission planners carefully decide on a safe routs for the rover avoiding obstacles of any kind that might get in its way. Eliminating all possible pitfalls scenarios might not be possible; however, elimination the likelihood or devising tools to remedy some of these scenarios is a must. The Spirit and Opportunity rovers were designed to explore at least a 600 m from the landing location (Townsend et al., 2014). Naturally, one of the future missions in preparation for the ultimate goal of human mission to Mars is to expand the exploration areas. In a recent paper by Toups et al., (2016), the authors described the current status of the zones on which human would likely land and live on the Martian surface; these zones are termed as 'Exploration Zones' (EZ); according to NASA, the Exploration Zones are area located within a 100 km from the landing site (Toups et al., 2016). Consequently, more challenges have to be faced and have to be addressed. Although the mission planners carefully select the routes through which the rovers traverse; however, increasing the exploration area would definitely require increasing the traversing speed. For example, Opportunity and its twin Spirit average speed is one centimeter per second (0.3937 inches per second). One of the undesirable scenarios that are likely to happen during any exploration mission is falling down on a soft soil during motion. The likelihood of such a scenario is high considering the fact that these rovers traverse on unknown terrains during planetary missions. The cost and efforts associated in the development, deployment and operating of these rovers dictate maximising the time available for exploration process. Thus, understanding the dynamics of falling on the plant's soft soil is the first step in the investigation of how to get the rover back in track. As mentioned above, the need for exploration of a wide area on planets surfaces requires the use of high-speed rovers; naturally, this would increase the chances of falling to lower levels. This case motivates the study of the dynamic response of such a fall on a soft soil and to understand the dynamic mechanics of a rigid wheel penetration into soft soil.

Wheel sinkage governs the dynamics and mobility of planetary vehicles. Planetary vehicles have metal rigid wheels to sustain the low temperatures on planets. In general, the size of rovers and their wheels are relatively small. High-speed motion of any vehicle encounters a fall down to a lower level of terrain. The fall becomes more severe especially if the ground is a soft soil. The gained knowledge of the interaction between rigid wheels - soil enhances the design of future planetary vehicles.

The theoretical investigation presented in this manuscript is part of an undergoing bigger scope project at the university. The long-term objectives of this project are to enhance the maneuverability and traction of a smart robot on uneven, soft soil similar to the terrains encountered in planetary exploration missions. This is an ongoing research area motivated by NASA's ambitions to inhabit the Red Planet by the year 2030s. The proposed research is focused on investigating methods to enhance the stability of the rover on loose soil using special wheel profile designed to increase the soil compactness along the rover's path.

The focus of the current stage of the project is to experimentally investigate the interaction of robot's wheels with soft soil during steering and turning around curves. To accomplish this task, a sand testbed is being designed to imitate the soft soil terrain on the plant's surface. The testbed is designed to allow measurements of the torques and forces between the wheels and the loose soil while moving forward, backward, or during steering when changing direction. The testbed is also designed to allow tilting right and left, which enables testing the rover's performance on uneven terrain.

Based on the experimentally validated optimal wheel features of the previous stage, the second major stage the project which will be carried out. The tasks will involve the design and build of a smart robot. From the manoeuvrability point of view, the smart robot is designed such that it can move simultaneously and independently in translation and rotation. The design enables the forward and the backward motions without changing wheels' direction, and it can also spin about a point, and drive a long any curve, or turn in any sharp angle.

2 Wheel-soft soil interaction mechanics

Off-road performance, efficiency and mobility of manned and unmanned vehicles rely primarily on the interaction between running wheels and soil. The mobility of the vehicle is a function the thrust and resistance forces produced at the interface. Moving on a soft soil tracks is not only a function of the state of the wheel, like road-vehicles applications, but also on the state of the soil underneath.

The field of terramechanics covers the interaction mechanics between wheel and soft terrain. The earlier studies in this field were focused on heavy duty machinery for agricultural and military applications (Bekker, 1956, 1960, 1969). Based on Bekker's findings, many studies, both theoretical and experimental, have been conducted to study the interaction mechanics of rigid wheel and soft soil for off-road vehicles. An explicit analytical form to estimate the wheels sinkage in a soft terrain was presented by Ding et al. (2015). Simulation and experimental validation terramechanics model for small-wheeled vehicles was presented by Meirion-Griffith et al. (2014) and Meirion-Griffith and Spenko (2014). Numerical simulations' results of the soil-wheel interaction were presented by Wakui and Terumichi (2010). There are many other similar studies that addressed this subject such as Meirion-Griffith and Spenko (2014), Taheri et al. (2015), Wong, (1983, 2014), Zhang et al. (2009) and Ziani and Biarez (1990).

In 1956 Bekker (1956) derived the analytical relationship of the normal stress σ exerted on a point on the rim of a wheel as function of the depth of point sinkage z for sandy soil; it represents the depth that a wheel will sink into the soil; thus, it signifies, and the resistance it will face during driving. The relationship is given by

$$\sigma = \left(k_1 + k_2 b\right)\left(\frac{z}{b}\right)^n \tag{1}$$

and the shear stress τ represents the traction that the wheel will generate when driven on the soft soil terrain. The relationship is given by

$$\tau(\theta) = \left(c_o + \sigma \cdot \tan\phi\right)\left(1 - e^{-j/k}\right) \tag{2}$$

where the sinkage exponent, n, signifies the nonlinear behavior of the curvature of the pressure-sinkage curve for a soil deformation, $k_1\left[KPa\right]$, and $k_2\left[\frac{KN}{m^3}\right]$ are the pressure sinkage moduli, r is wheel radius [m], b is wheel width [m], j shear deformation distance, ϕ is internal friction angle [deg], k is the shear deformation modulus and c_o is the soil cohesion.

Based on previous experiments using sand to represent the soft soil terrain, it has been shown that the location of the maximum normal stress is a function of the slip I (Senatore and Iagnemma, 2014), where the slip is defined as

$$i = 1 - \frac{\text{actual traveling speed}}{\text{wheel linear speed}} \tag{3}$$

The angular position of the maximum normal stress, θ_m, on a rim of rigid wheel has been thoroughly investigated by many researchers (Senatore and Iagnemma, 2014; Wong & Reece, 1967). As shown in Figure 1, θ_m is given by a linear relationship

$$\theta_m = \left(c_1 + c_2 i\right)\theta_1 \tag{4}$$

Figure 1 Free body diagram of driven rigid wheel on soft soil, profiles of normal and shear stresses

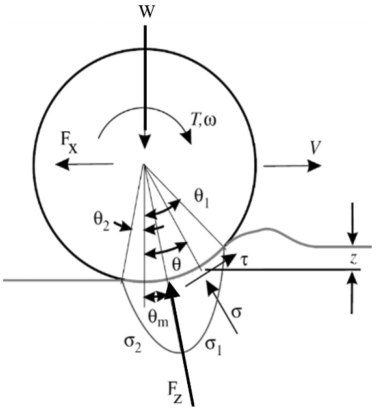

Soruce: Shibly et al. (2005)

where c_1 and c_2 are the coefficients that define the relative location of the maximum normal stress and θ_1 is the angular location of during rotation of the wheel, each point on the contact surface of the rim and the soil has sinkage z. The sinkage is determined as the difference between the vertical projections of the locations of the point of interest and the

first contact point which leads to the conclusion that the sinkage z is a function of angular position θ and the radius of the wheel, r.

The normal stress distribution given in Eq. (1) can be expressed as a function of the angular position θ using the unique relationship between sinkage and angular location of any point on the wheel's rim.

Substituting this relation into Eq. (1) gives the distribution of the normal stress along the contact surface as

$$\sigma_1(\theta) = (k_1 + k_2 b)\left(\frac{r}{b}\right)^n (\cos\theta - \cos\theta_1)^n \tag{5}$$

$$\sigma_2(\theta) = (k_1 + k_2 b)\left(\frac{r}{b}\right)^n \left[\cos\left(\theta_1 - \frac{\theta + \theta_2}{\theta_m + \theta_2}(\theta_1 - \theta_m)\right) - \cos\theta_1\right]^n \tag{6}$$

Equation (5) is defined in the range $\theta_m \le \theta \le \theta_1$, while Eq. (2) is defined in the range $\theta_2 \le \theta \le \theta_m$ as illustrated in Figure 1. The stress indices in the equations are referred to the zone number.

The normal stress around the wheel's rim starts from zero at the free surface, at the starting point of the contact area, increases toward a maximum value and then decreases back to zero at the end of contact with soil as demonstrated by Harnisch et al. (2005), Hathorn et al. (2014), Law and Wong (1994), Meirion-Griffith and Spenko (2011b, 2013), Wong and Reece (1967) and Ziani and Biarez (1990). This stress distribution is divided into two zones as shown in Figure 1.

Determination of the total shear deformation distance j of a point on the wheel's rim which slips in soft soil was introduced by Harnisch et al. (2005), Wong and Reece (1967) and Yong and Windisch (1970) as

$$v_j = r\omega - v_{\text{wheel axis}}\cos\theta = r\omega\left[1 - (1-i)\cos\theta\right] \tag{7}$$

$$j = \int_0^t v_j dt = \int_{\theta_1}^{\theta} r\left[1 - (1-i)cos\theta\right] d\theta$$

$$j = r\left[\theta_1 - \theta - (1-i)(\sin\theta_1 - \sin\theta)\right] \tag{8}$$

Upon substitution of this expression into Eq. (2), the shear stress during slippage can be expressed as

$$\tau(\theta) = (c_o + \sigma \cdot \tan\phi)\left(1 - e^{-\frac{r}{k}\left[\theta_1 - \theta - (1-i)(\sin\theta_1 - \sin\theta)\right]}\right) \tag{9}$$

where c_o is the soil cohesion, ϕ is the angle of internal friction and k is the shear modulus coefficient.

Another approach was taken to determine the shear deformation distance j by considering the path of any point on the wheel's rim as cycloid and is function of the slippage (Janosi, 1961; Salama and Vantsevich, 2013; Taheri et al., 2014; Wulfsohn and Upadhyaya, 1991) [5]. The result is more complicated expression. In this work, the shear deformation distance j given in Eq. (7) is adopted.

Upon determination of the normal and shear stresses profiles, the forces and the torques that act on the contact surface of a rigid wheel during driving on a soft terrain can be determined by integration as follows:

The horizontal component of the stresses are integrated to give the horizontal force F_x,

$$F_x = rb\left(\int_{\theta_2}^{\theta_1}\tau(\theta)\cos\theta\cdot d\theta - \int_{\theta_2}^{\theta_1}\sigma(\theta)\sin\theta\cdot d\theta\right) \tag{10}$$

While the vertical components of the stresses to give the vertical force F_z,

$$F_z = rb\left(\int_{\theta_2}^{\theta_1}\sigma(\theta)\cos\theta\cdot d\theta + \int_{\theta_2}^{\theta_1}\tau(\theta)\sin\theta\cdot d\theta\right) \tag{11}$$

and finally the shear stress on the contact area to give the torque T, as follows:

$$T = r^2 b\int_{\theta_2}^{\theta_1}\tau(\theta)\cdot d\theta \tag{12}$$

The nonlinearity of j expression in the shearing stress formula in Eqs. (9)–(11) forced numerical integration in order to determine the forces and torque. In this case, there is no closed-form solution for the forces and torque that act on a wheel while interacting with soft soil. The absence of closed-form solution prevents mathematical operation of the wheel equilibrium equations which is needed for the online wheel-soil interaction prediction as it happens in the case of planetary missions. The online soil characteristics prediction requires another approach of forces and torque evaluation (Shibly et al., 2005).

A previous work on reformulation of the basic mechanics of a rigid-driven wheel on a soft terrain was introduced by Iagnemma et al. (2002) and Shibly et al. (2005). Recalculating the stress distribution around the rim of a driven rigid wheel that is based on the experimental data given in Law and Wong (1994) and redrawing of the normal and shear stresses distributions on a Cartesian Coordinates axis yields pattern very close to a triangular distribution as illustrated in Figure 2.

Figure 2 (a) and (b) Normal stress and shear stress distribution around the rim of driven rigid wheel on soft terrain for different values of *n*. (c) and (d) the same as in (a) and (b) with the stress equivalent distribution (see online version for colours)

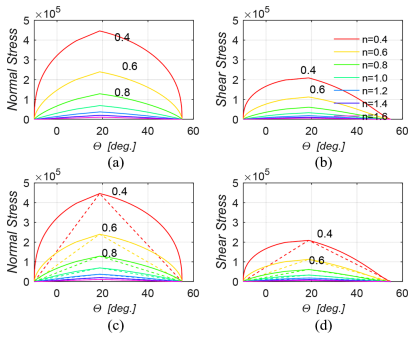

Source: Shibly et al. (2005)

Least-squares regression analysis of the stresses distribution around the rigid wheel during interaction with a soft soil leads two expressions for the normal and shear stresses shown in Eq. (13). The objective of these modification is extend the triangular approximate stress distribution shown in dashed lines in Figure 2 so that the areas under real normal and shear stress distribution curves for a given soil index n and the modified approximate distribution are equal as depicted in Figure 3. The two modifying factors for the normal stress and shear stress distribution were found as function of the soil exponent n, respectively, as

$$\text{fac}_{\text{ns}} = -0.49n + 1.6683$$

$$\text{fac}_{\text{ss}} = 0.1381n + 0.815 \tag{13}$$

Figure 3 Stress distribution and its equivalent distribution around the rim of driven rigid wheel on soft terrain for different values of soil exponent n. (a) Normal stress and (b) Shear stress (see online version for colours)

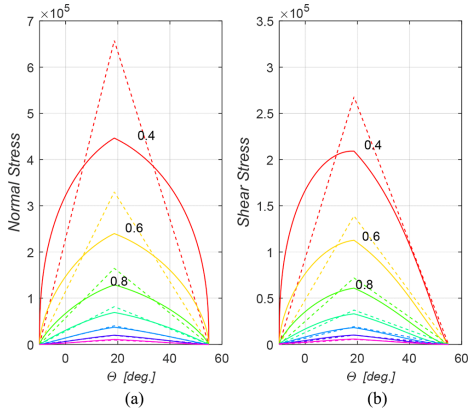

The relative error of the stresses distribution areas for various exponential soils n is shown in Figure 4. The maximum relative error is obtained by Eq. (13), and the true stress distribution is less than 0.4%.

Figure 4 Relative error of the equivalent stress distribution with the modified height around the rim of driven rigid wheel on soft terrain for different values of n (see online version for colours)

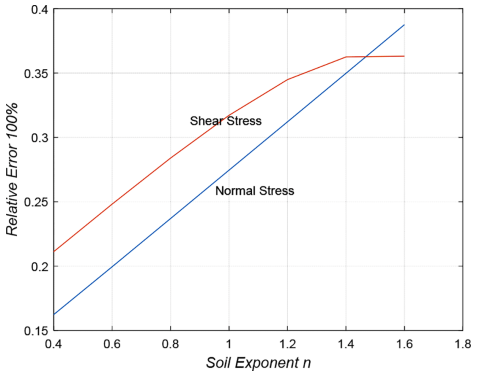

These results would justify using the approximate triangular normal and shear stresses distributions. This observation has been investigated and adopted by several researchers such as Meirion-Griffith and Spenko (2011a), Vincent (1961), Wulfsohn and Upadhyaya (1991), and Ziani and Biarez (1990).

The normal force F_z shown in Figure 1 can be found by integration of the normal stress and the sheer stress acting on the rim of a rigid wheel that is interacting with soft soil to give the normal force as

$$F_z = rb\left(\int_{\theta_m}^{\theta_1}\left(\sigma_1(\theta)\cos\theta+\tau_1(\theta)\sin\theta\right)d\theta+\int_{\theta_2}^{\theta_m}\left(\sigma_2(\theta)\cos\theta+\tau_2(\theta)\sin\theta\right)d\theta\right) \tag{14}$$

Due to the nonlinearity in the normal stress and shear stress expressions formula given in Eqs. (5), (6) and (9), the integration has to be carried out numerically. The stress distribution can be approximated by an equivalent triangle, which has the same area and the same maximum stress value with θ_1 as its base. Based on this approximation, the equivalent stresses distribution that acts on the wheel contact surface with soft soil has been developed. Consequently, a new closed-form formulation of the rigid wheel-soft soil interaction mechanics has been developed. A comparison between these two approaches was compared with conventional formulations for analysis of forces and torques that act on the wheel. The results of the comparison shown graphically were very closely correlated. An experimental validation of the theoretical results was presented (Shibly et al., 2005).

3 Stresses and forces analysis

As mentioned in the previous section, the equivalent triangular distribution for the two stress zones depicted in Figure 1 yields a linear stress distribution. The equivalent stress distribution S_{ni} and S_{ti} of normal stress σ and shear stress τ are triangles with two sides are defined by

$$S_{n1}(\theta)=\frac{\theta_1-\theta}{\theta_1-\theta_m}S_{nm},\ S_{n2}(\theta)=\frac{\theta_2+\theta}{\theta_2+\theta_m}S_{nm} \tag{15}$$

and

$$S_{t1}(\theta)=\frac{\theta_1-\theta}{\theta_1-\theta_m}S_{tm},\ S_{t2}(\theta)=\frac{\theta_2+\theta}{\theta_2+\theta_m}S_{tm}-\frac{\theta-\theta_m}{\theta_2+\theta_m}S_{t2}(\theta_2) \tag{16}$$

where the indices 1 and 2 refer to the right and left sides relative to the maximum stress respectively.

Based on the above stress and force analysis, the dynamic response of the rover after free fall in soft soil is investigated. Such a scenario is expected in any planetary exploration mission, as well as unmanned and manned ground vehicles. Depending on the severity of the fall, the vehicle undergoes different stages that involve sinkage of the rotating rigid wheel in the soil, pulling out from the soil as described before. To simplify the analysis of the wheel-soft soil interaction, the wheel is assumed to be clamped to prevent it from rotation. Such a simplification facilitates the study of dynamic behavior of the rover. This arrangement is similar to the interaction of walking robot foot and a soft

soil. The shape of the foot in this study is circular and has the same radius as of the wheel. Using this assumption, the normal stress during sinkage stage as function of the wheel sinkage has symmetric distribution in both sides of the vertical direction, and the location of maximum stress is at the lowest point of the wheel as shown in Figure 5.

Figure 5 (a) Free body diagram of rigid wheel on soft soil and (b) Equivalent triangular distribution of normal stresses (see online version for colours)

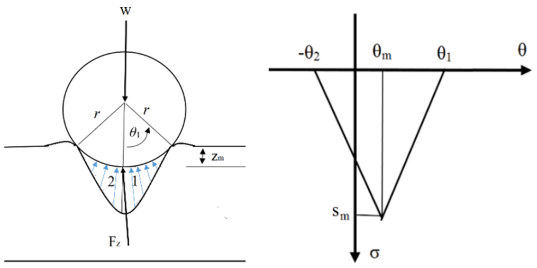

(a) (b)

The equivalent distribution in this case is an isosceles triangle where $\theta_2 = -\theta_1, \theta_m = 0$. Upon substitution of the equivalent stress distribution and evaluating the integral of the normal stress, it can be found as

$$F_z = 2rb\left(\int_0^{\theta_1} \sigma_1(\theta)\cos\theta \cdot d\theta\right) \tag{17}$$

The vertical force F_z can then be found by substitution of Eqs. (15) and (16) into Eq. (17) as

$$F_z = rb\sigma_m\left(2\frac{1-\cos\theta_1}{\theta_1}\right) \tag{18}$$

The fitted straight line to the parenthetical expression in Eq. (18) as θ varies between 0 and 45°, has a 0.98 gradient; consequently, the expression can be further simplified as shown in Eq. (19).

$$2\frac{1-\cos\theta_1}{\theta_1} \cong 0.98\theta_1 \tag{19}$$

From geometry shown in Figure 5:

$$1-\cos\theta_1 = \frac{z_m}{r} \tag{20}$$

Equating Eqs. (19) and (20), a more simplified relationship between the entry angle θ_1 and a maximum sinkage z_m

$$\theta_1 = \sqrt{\frac{fz_m}{r}}, \text{ where } f = 2.0408 \tag{21}$$

Then, the normal force F_z can be obtained as

$$F_z = rb\sigma_m\sqrt{\frac{fz_m}{r}} \tag{22}$$

The maximum value of normal stress is at $\theta = 0°$. Upon substitution in Eq. (4) to get

$$\sigma_m = \sigma_1(0) = (k_1 + k_2 b)\left(\frac{r}{b}\right)^n (1-\cos\theta_1)^n \tag{23}$$

After considerable simplifications, the normal force can be obtained as

$$F_z = (k_1 + k_2 b)\left(\frac{\sqrt{fr}}{b^{n-1}}\right)(z_m)^{n+\frac{1}{2}} \tag{24}$$

The last expression of the vertical force F_z shows that the normal force is a function of the sinkage z_m during penetration in the soil. This function is highly nonlinear, and it can be further simplified. For a specific wheel-soil parameters, the coefficient of the sinkage has constant value k_z which is defined as follows:

$$k_z = (k_1 + k_2 b)\left(\frac{\sqrt{f \cdot r}}{b^{n-1}}\right) \tag{25}$$

k_z can be defined as the stiffness modulus of the soil in the vertical direction, and then Eq. (25) can be rewritten as function of the sinkage and the soil exponent n as

$$F_z = k_z (z_m)^{n+\frac{1}{2}} \tag{26}$$

Based on the above simplifications, the normal sinkage resistance force F_z as function of the sinkage z_m for various values of soil sinkage exponent n is shown in Figure 6. Typical values of different terrain soils can be found in Wong (2010), for example. The general trend of the stiffness modulus k_z is to increase as the soil sinkage increases.

Figure 6 Normal sinkage resistance force of soil as function of sinkage for various values of soil exponent n (see online version for colours)

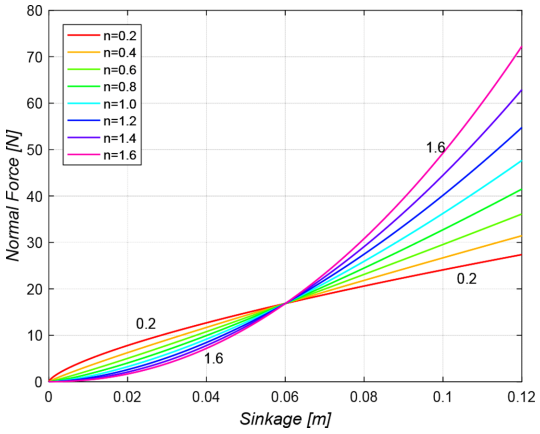

4 Kinematic model of four wheels rover

Four-wheel planetary vehicle (rover) has a mechanical structure (suspension) between its platform and the four wheels. In this work, a simplified quarter-car vehicle model is considered. The linear model captures basic performances of rover such as body displacement, body acceleration and wheel displacement. The model has a lumped sprung mass m_s representing one quarter of the rover body mass attached to a rigid wheel through a mechanical suspension. The rigid wheel is modelled as another lumped unsprung mass m_{us} with radius *r*. The proposed suspension system is modelled as a vertical linear spring with high stiffness k_s and a linear damper with low damping coefficient c_s. The proposed schematic model is shown in Figure 7.

Figure 7 Dynamic model of quarter rover

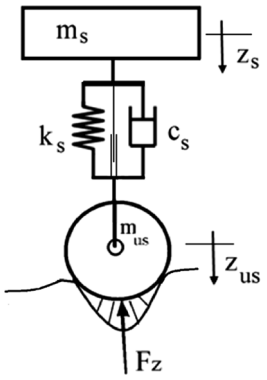

5 Dynamics response analysis

The dynamic response of the rover caused by its free fall on soft ground starts at the time that the wheel touches the ground and ends when the wheel leaves the ground starting the second cycle of oscillation.

The dynamic equation of motion of a quarter rover at the instant of first ground contact starts with zero initial positions and with initial velocity equal to the final velocities of the free fall.

Using Newton's second law for the sprung mass m_s, and for the wheel, m_{us}, the governing equations of motion for the model under consideration are obtained as shown in Eqs. (27) and (28).

$$m_s \ddot{z}_s + c_s\left(\dot{z}_s - \dot{z}_{us}\right) + k_s\left(z_s - z_{us}\right) = m_s g \tag{27}$$

$$m_{us} \ddot{z}_{us} + c_s\left(\dot{z}_{us} - \dot{z}_s\right) + k_s\left(z_{us} - z_s\right) = m_{us} g - F_z \tag{28}$$

These equations can be expressed in matrix form as

$$M\ddot{Z} + C\dot{Z} + KZ = F \tag{29}$$

Where:

$$Z=\begin{bmatrix} z_s \\ z_{us} \end{bmatrix}, M=\begin{bmatrix} m_s & 0 \\ 0 & m_{us} \end{bmatrix}, C=\begin{bmatrix} c_s & -c_s \\ -c_s & c_s \end{bmatrix}, K=\begin{bmatrix} k_s & -k_s \\ -k_s & k_s \end{bmatrix}, F=\begin{bmatrix} m_s g \\ m_{us} g - F_z \end{bmatrix} \quad (30)$$

The damping coefficient of the rover structure system is considerably small; therefore, it can be assumed that it will not have a significant effect on the natural frequencies of the suspension structure and can be neglected for the purpose of determining the eigenvalues and eigenvectors (Clough and Penzien, 1975). Based on this approximation, the eigenvalues and eigenvectors of the proposed model:

$$det\left(K-\omega^2 M\right)=0 \quad (31)$$

The eigenvalues and the associated eigenvectors of the simplified model can be obtained, respectively, as

$$\lambda_1=\omega_1^2=0,\ \lambda_2=\omega_2^2=\frac{k_s}{\mu},\ \text{where}\ \mu\ \text{is the reduced mass},\ \mu=\frac{m_s m_{us}}{m_s+m_{us}} \quad (32)$$

The associated eigenvectors are, respectively,

$$\phi_1=\begin{Bmatrix} 1.00 \\ 1.00 \end{Bmatrix},\ \phi_2=\begin{Bmatrix} 1.00 \\ -\eta \end{Bmatrix},\ \text{where}\ \eta=\frac{m_s}{m_{us}}. \quad (33)$$

This combination of eigenvalues and eigenvectors shows that the first normal mode shapes the two masses move in-phase as a rigid body, while the second normal mode shapes the two masses move out of phase with amplitude ratio of η.

Considering the conditions at the end of phase two and solving the equation of motion to achieve the condition for the occurrence of the third phase, the condition for the acceleration of the mass m_s should have acceleration as shown in Eq. (34).

$$\ddot{z}_s \geq \left(1+\frac{1}{\eta}\right) g \quad (34)$$

The equations of motion are solved numerically, and the simulation results for velocity, displacement and the normal sinkage resistance force are shown in Figures 8–10, respectively.

Figure 8 depicts the displacement of the rover body and the wheel at successive stages of the interaction for a given set of parameters that include soil exponent n and the wheel width. Point 1 in part a of the figure represents the instant at which the wheel touches the soft soil. At this point, the system has an initial velocity of the free falling body, and the datum for the displacement is taken to be zero at this point. Point 2 denotes the maximum sinkage of the wheel at which the wheel velocity is zero as shown in Figure 9. Point 3 represents the beginning of the second cycle of the response; at this point, the system starts to pull out of the soil and then go back again at point 4. Note that the depth of sinkage decreases with time. Part b of Figure 8 characterises the response of the same system considered in part a, however, considering a small damping coefficient. Note that the oscillatory behaviour of the unsprung mass is almost suppressed.

Figure 8 The displacements of the sprung mass z_s and the wheel z_{us} during time, (a) undamped system and (b) damped system (0.3 damping ratio) (see online version for colours)

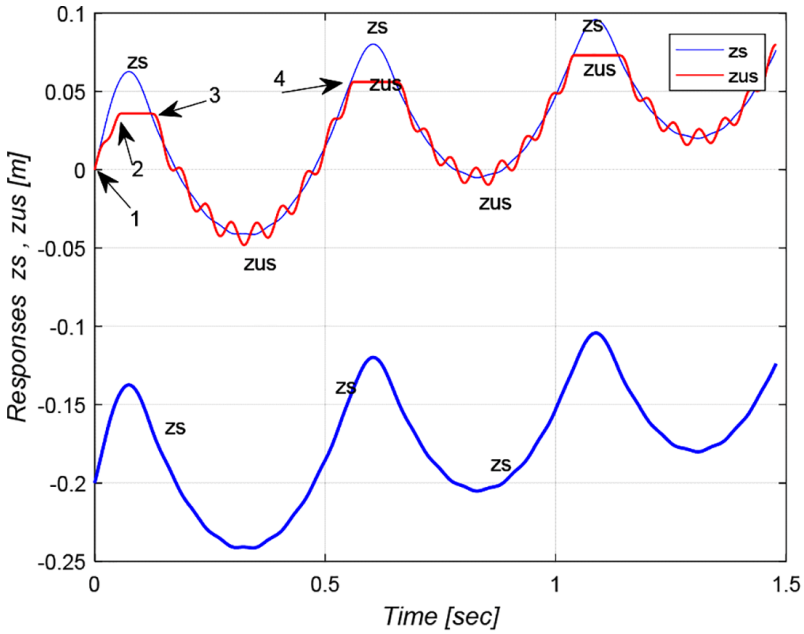

(a)

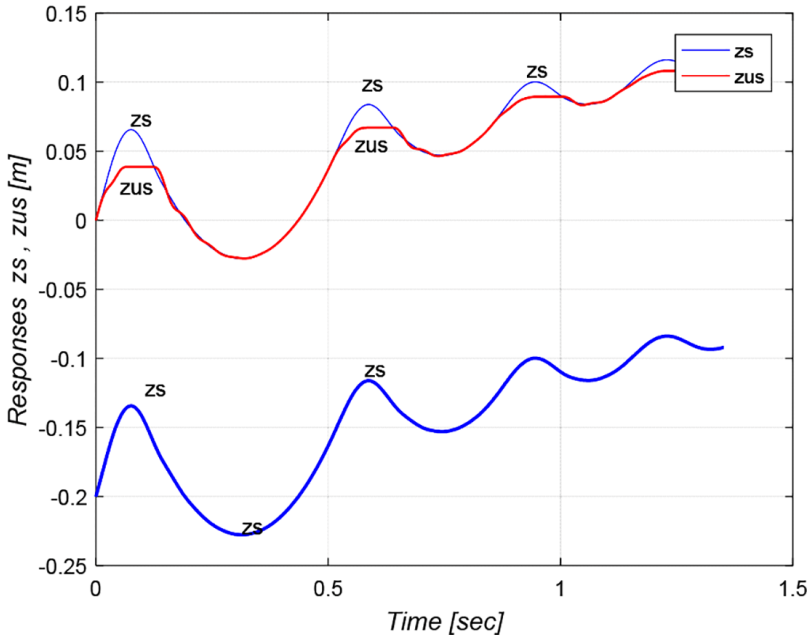

(b)

Figure 9 The velocities of the sprung mass v_s and the wheel v_{us} vs time. (a) undamped system and (b) damped system (0.3 damping ratio) (see online version for colours)

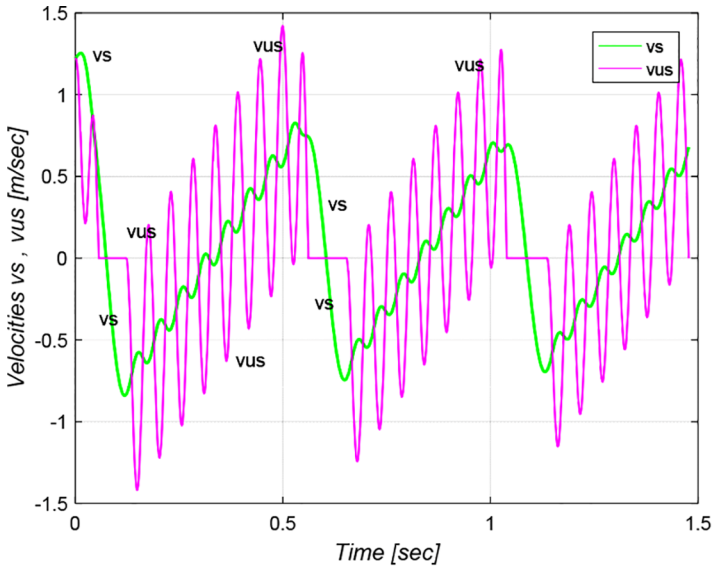

(a)

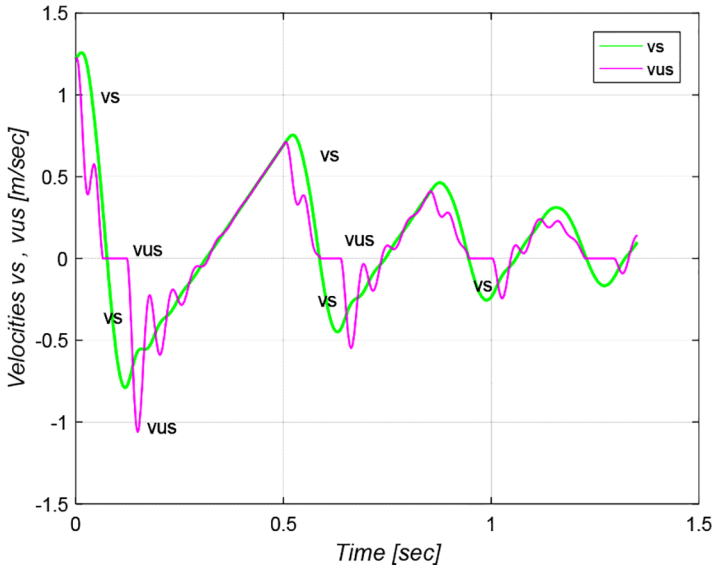

(b)

Figure 9a illustrates the velocities of the sprung and the unsprung masses neglecting the damping. Part b of Figure 9 shows the velocities considering a lightly damped system.

Figure 10 depicts the resistance forces F_z for a particular set of the system parameters. As expected, the value of the resistance force decreases as the intensity of the interaction between the wheel and the soil decreases. As shown, part a represents an undamped case, and part b represents the lightly damped case.

Figure 10 The normal resistance force as function of time for, (a) undamped system and (b) damped system (0.3 damping ratio) (see online version for colours)

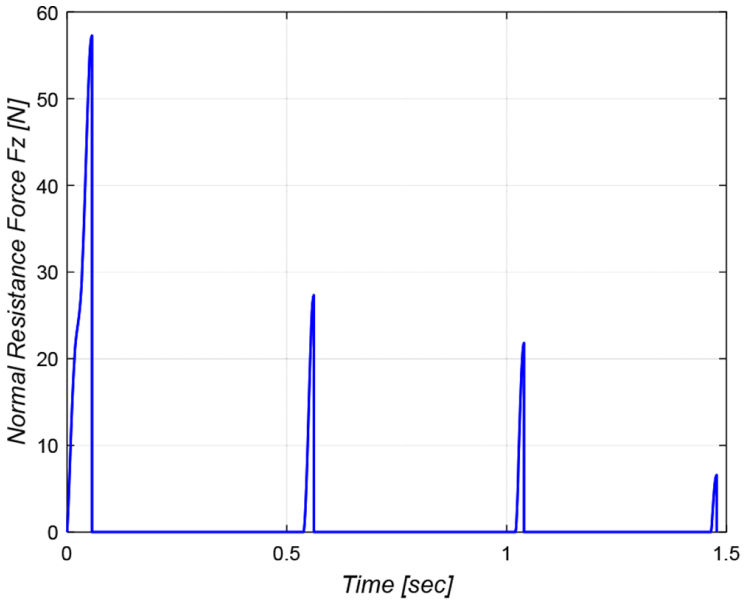

(a)

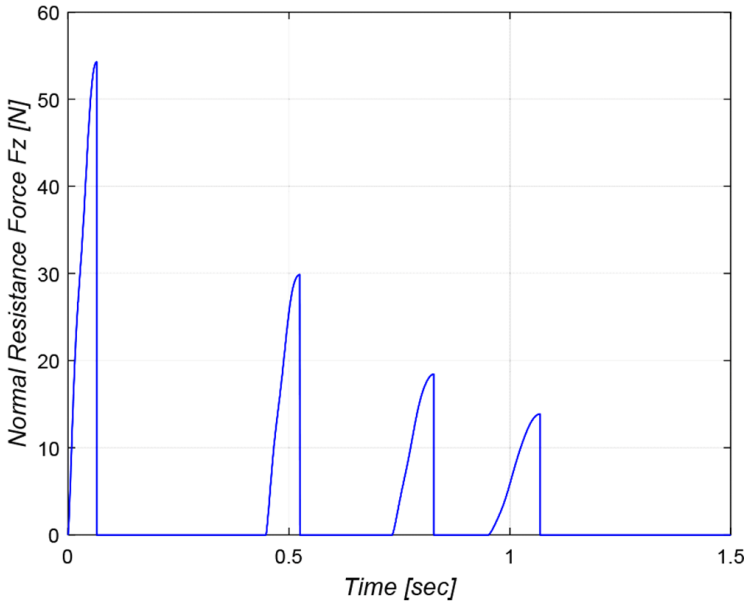

(b)

To investigate the effect of damping on the sinkage resistance force F_z, two more simulations were carried out as shown in Figure 11. The effect of the increase in the damping coefficient is evident on the value of the sinkage resistance force as shown.

Figure 11 (a) Damped system 0.7 damping ratio and (b) overdamped system (see online version for colours)

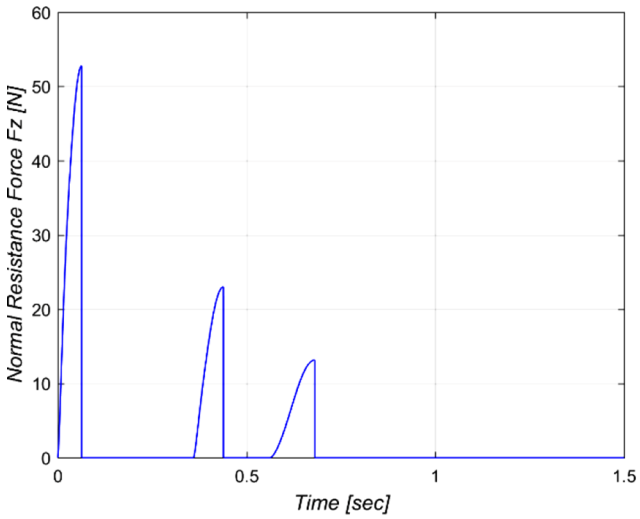

(a)

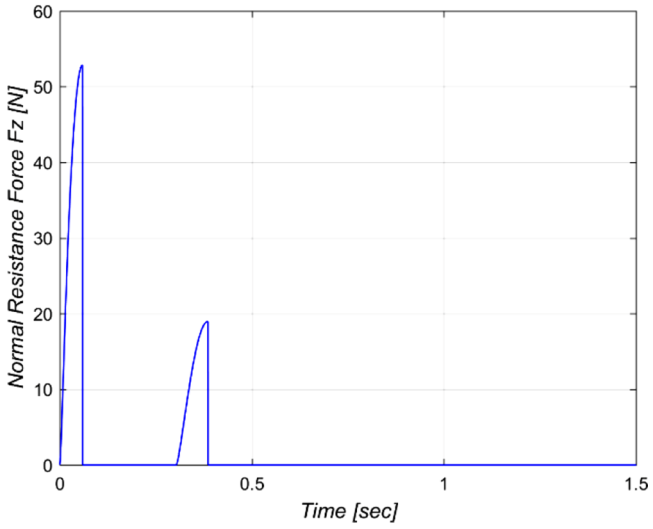

(b)

6 Results and discussion

Comparing the coefficient k_z and the normal sinkage resistance force F_z for a two different values of soil exponent n, the first ratio and the second ratio are obtained as shown in Eqs. (35) and (36) respectively

$$\frac{k_z(n2)}{k_z(n1)} = (b)^{n1-n2} \tag{35}$$

$$\frac{F_z(n2)}{F(n1)} = \left(\frac{z}{b}\right)^{n2-n1} \tag{36}$$

the two ratios for soil coefficients value $n_1 = 0.2$, $n_2 = 1.6$ and wheel width of $b = 0.06m$ was found to be 51.36 for the coefficient k_z, the ratio of normal sinkage resistance force F_z for a sinkage value of =b/2, (at maximum difference between normal forces) is only 0.379 times. This means that the soil exponent *n* has a significant effect on the coefficient k_z though this effect is been minimised in the formula of the normal sinkage resistance force.

The relative deviation from a straight line behaviour of the soil normal sinkage resistance force as function of sinkage depth is very large. The intersecting point occurs at sinkage value equal to the wheel width b. At this point, the effect of the soil exponent *n* is nullified. Therefore, the soil reaction during sinkage may be considered as a non-linear spring with constant coefficient of stiffness k_z.

The interaction between the rigid wheel (unsprung mass) and soft soil has three stages. At each stage, the force F_z is different. During the first stage, between points 1 and 2 as depicted in Figure 9a, where the wheel penetrates in the soft soil until it reaches its maximum sinkage at zero velocity. At this stage, the sinkage resistance force F_z reaches its maximum value and is calculated according to the expression given in Eq. (26). The second stage starts at maximum sinkage and ends at the instant of disengagement from the soil, between points 2 and 3 as illustrated in Figure 9a. The wheel velocity at this stage is zero, and the normal force on the wheel is the reaction force to all other forces that act on the wheel. The third stage starts when the sprung mass has acceleration as given in Eq. (34) be able to pull up the unsprung mass (wheel), then the wheel losses contact with the soil and it is between points 3 and 4 as shown in Figure 9a. During this stage, the normal force is zero and the system starts to vibrate according to its two eigenvectors with an initial condition equal to the motion parameters at the end of stage 2.

It can be noticed that there is a significant effect of the rigid body mode at the starting of stage 3. This mode helps in pulling up the wheel from the sinkage as shown in Figure 9.

At the first stage, the penetration linearly increases with time as shown in Figure 9, and the wheel penetration speed is influenced by the normal projection of soil stresses on the wheel's rim, and the suspension forces are caused by the sprung mass, which are pushing down in the direction of motion.

The first fall makes the soil more compact, as a result, the soil parameters are changed and the sinkage is much less than the first time, and it is harder to penetrate in. In case, the wheel is not bouncing back that the sprung mass will continue to vibrate about its final position.

The damping in the suspension dissipates energy and reduces the oscillation speed which results in a longer wheel-soil penetration time and earlier occurrence of successive penetrations as shown in Figures 10 and 11.

Adding damping to the system reduces the vibration of both sprung mass and unsprung mass (wheel) significantly. Also the maximum value of the force in the second sinkage is much less than the first one. The damper is very essential if the fall occurs on

earth as it is expected, but in space, it is preferred not to have damper and let the masses bounce up to have the wheel bouncing up and to get released from the soil.

The normal force behaviour during sinkage and contact with soil happens during very short time, and it has a geometric-shaped resemblance to any impulsive force during collision of two objects; therefore, a future work is to replace the sinkage force with an impulse applied to the wheel during contact with the soil.

References

Bekker, G.M. (1956) *Theory of Land Locomotion: The Mechanics of Vehicle Mobility*, University of Michigan Press, Ann Arbor.

Bekker, G.M. (1960) *Off-The-Road Locomotion: Research and Development in Terramechanics*, University of Michigan Press, Ann Arbor.

Bekker, G.M. (1969) *Introduction to Terrain-Vehicle Systems*, University of Michigan Press, Ann Arbor.

Clough, R.W. and Penzien, J. (1975) *Dynamics of Structures*, McGraw Hill, New York.

Ding, L., Haibo, G., Yuankai, L., Guangjun, L. and Zongquan, D. (2015) 'Improved explicit-form equations for estimating dynamic wheel sinkage and compaction resistance on deformable terrain', *Mechanism and Machine Theory*, Vol. 86, pp.235–264. doi:10.1016/j.mechmach theory.2014.12.011

Harnisch, C., Lach, B., Jakobs, R., Troulis, M. and Nehls, O. (2005) 'A new tyre-soil interaction model for vehicle simulation on deformable ground', *Vehicle System Dynamics*, Vol. 43, pp.384–394. doi:10.1080/00423110500139981

Hathorn, G.N.B., Blackburn, K. and Brighton, J.L. (2014) 'An investigation into wheel sinkage on soft sand', *Tire Science and Technology*, Vol. 42, No. 2, pp.85–100.

Iagnemma, K., Shibly, H. and Dubowsky, S. (2002) 'On-line terrain parameter estimation for planetary rovers', *Paper presented at the 2002 IEEE International Conference on Robotics Adn Automation*, 11 May 2002–15 May 2002, Washington, DC, USA.

Janosi, Z. (1961) 'An analysis of pneumatic tire performance on deformable soils', *Paper presented at the First International Conference on Terrain Vehicle Systems*, Torino.

Law, E.H. and Wong, J.Y. (1994) 'Theory of ground vehicles', *Journal of Terramechanics*, Vol. 31, No. 6, pp.415–415. doi:10.1016/0022-4898(94)90026-4

Meirion-Griffith, G., Nie, C. and Spenko, M. (2014) 'Development and experimental validation of an improved pressure-sinkage model for small-wheeled vehicles on dilative, deformable terrain', *Journal of Terramechanics*, Vol. 51, No. 1, pp.19–29. doi:10.1016/j.jterra.2013. 11.003

Meirion-Griffith, G. and Spenko, M. (2011a) 'A modified pressure-sinkage model for small, rigid wheels on deformable terrains', *Journal of Terramechanics*, Vol. 48, No. 2, pp.149–155. doi:10.1016/j.jterra.2011.01.001

Meirion-Griffith, G. and Spenko, M. (2011b) 'Toward establishing a comprehensive pressure-sinkage model for small diameter wheels on deformable terrains', *Paper presented at the 17th International Conference of the International Society for Terrain Vehicle Systems 2011, ISTVS 2011*, 18 November 2011 – 22 November 2011, Blacksburg, VA, USA.

Meirion-Griffith, G. and Spenko, M. (2013) 'A pressure-sinkage model for small-diameter wheels on compactive, deformable terrain', *Journal of Terramechanics*, Vol. 50, No. 1, pp.37–44. doi:10.1016/j.jterra.2012.05.003

Meirion-Griffith, G. and Spenko, M. (2014) 'Simulation and experimental validation of a modified terramechanics model for small-wheeled vehicles', *International Journal of Vehicle Design*, Vol. 64, Nos. 2–4, pp.153–169. doi:10.1504/IJVD.2014.058499

Salama, M. and Vantsevich, V.V. (2013) 'Tire-terrain normal and longitudinal dynamics and slip power losses of an unmanned ground vehicle', *Paper presented at the ASME 2013 International Mechanical Engineering Congress and Exposition, IMECE 2013*, 15 November 2013–21 November 2013, San Diego, CA, USA.

Senatore, C. and Iagnemma, K. (2014) 'Analysis of stress distributions under lightweight wheeled vehicles', *Journal of Terramechanics*, Vol. 51, No. 1, pp.1–17. doi:10.1016/j.jterra.2013.10.003

Shibly, H., Iagnemma, K. and Dubowsky, S. (2005) 'An equivalent soil mechanics formulation for rigid wheels in deformable terrain, with application to planetary exploration rovers', *Journal of Terramechanics*, Vol. 42, No. 1, pp.1–3. doi:10.1016/j.jterra.2004.05.002

Taheri, S., Sandu, C. and Taheri, S. (2014) 'Development and implementation of a hybrid soft soil tire model (HSSTM)', *Paper presented at the 18th International Conference of the International Society for Terrain-Vehicle Systems, ISTVS 2014*, 22 September 2014–25 September 2014, Seoul, Republic of Korea.

Taheri, S., Sandu, C., Taheri, S., Pinto, E. and Gorsich, D. (2015) 'A technical survey on Terramechanics models for tire-terrain interaction used in modeling and simulation of wheeled vehicles', *Journal of Terramechanics*, Vol. 57, pp.1–22. doi:10.1016/j.jterra.2014.08.003

Toups, L., Hoffman, S.J. and Watts, K. (2016) 'Mars surface systems common capabilities and challenges for human missions', *Paper presented at the 2016 IEEE Aerospace Conference, AERO 2016*, 5 March 2016–12 March 2016, Big Sky, MT, USA.

Townsend, J., Seibert, M., Bellutta, P., Ferguson, E., Forgette, D., Herman, J., Justice, H., Keuneke, M., Sosland, R., Stroupe, A. and Wright, J. (2014) 'Mars exploration rovers 2004-2013: evolving operational tactics driven by aging robotic systems', *Paper Presented at the 13th International Conference on Space Operations, SpaceOps 2014*, 5 May 2014–9 May 2014, Pasadena, CA, USA.

Vincent, E.T. (1961) 'Pressure distribution on and flow of sand past rigid wheel', *Paper presented at the First International Conference On Terrain Vehicle Systems*, Torino.

Wakui, F. and Terumichi, Y. (2010). 'Numerical simulation of tire behavior on soft ground', *Paper Presented at the 5th Asian Conference on Multibody Dynamics 2010, ACMD 2010*, 23 August 2010–27 August 2010, Kyoto, Japan.

Wong, J.Y. (1983) 'Introduction to terramechanics', *Journal of Terramechanics*, Vol. 21, No. 1, pp.5–17. doi:10.1016/0022-4898(84)90004-1

Wong, J.Y. (2010) *Terramechanics and Off-Road Vehicle Engineering*, Elsevier, Amsterdam.

Wong, J.Y. (2014) 'Terramechanics and its applications to the evaluation of terrestrial and extraterrestrial vehicle mobility: theory into practice', *International Journal of Vehicle Design*, Vol. 65, No. 4, pp.384–410. doi:10.1504/IJVD.2014.063834

Wong, J-Y. and Reece, A.R. (1967) 'Prediction of rigid wheel performance of driven rigid wheels, part I', *Journal of Terramechanics*, Vol.4, No. 1, pp.81–98.

Wulfsohn, D. and Upadhyaya, S.K. (1991) 'Traction of low-pressure pneumatic tires in deformable terrain', *Paper Presented at the International Off-Highway and Powerplant Congress and Exposition*, 9 September 1991–12 September 1991, Milwaukee, WI, USA.

Yong, R.N. and Windisch, E. (1970) 'Determination of wheel contact stresses from measured instantaneous soil deformations', *Journal of Terramechanics*, Vol. 7, Nos. 3–4, pp.57–67.

Zhang, X., Sun, B., Sun, Q. and Chen, N. (2009) 'Vehicle and terrain interaction based on Adams-Matlab co-simulation', *Journal of Southeast University (English Edition)*, Vol. 25, No. 3, pp.335–339.

Ziani, F. and Biarez, J. (1990) 'Pressure sinkage relationship for tyres on very loose sand', *Journal of Terramechanics*, Vol. 27, No. 3, pp.167–177. doi:10.1016/0022-4898(90)90009-B